Parameter Calibration of Chaboche Kinematic Hardening Model by Inverse Analysis Using Different Optimization Methods in the Case of Pipe Bending

Ozan Akkoyun[1] , İlyas Kacar[2,*]

[1] *Ditaş, Kayseri yolu 3.km 51100 Niğde, Turkiye,*
[2.]*Mechatronics Engineering, Engineering Faculty, Niğde Ömer Halisdemir University, Niğde, Turkiye,*

Abstract

Drag link is one of the important parts in steering system used in automotive. The ball joint, ball joint housing, and pipe compose the drag link. In this study, finite element analysis is used to simulate the deformation process. St 52 steel material is used. A yield criterion, an associated flow rule, and Chaboche's kinematic hardening rule were used in the finite element simulations of processes involving high plastic deformation. A series of low-cycle tensile/compression tests is performed to determine the parameters of Chaboche's kinematic hardening rule. The success of the simulation results depends on the more accuracy of the finding parameters. Some optimization methods are used in the calibration progression of these parameters and the results are compared. For the purpose of optimization, the angle of the pipe after bending is set as 16.6° as soon as possible. As design variables, the Chaboche kinematic hardening rule parameters were adjusted. Consequently, calibrated parameters were obtained for St52 pipe bending. By analysing and verifying the candidate points, optimization methods are compared. The optimum parameters are determined as YS=350 MPa, C=2984.3 MPa, and γ=100 while their initial values are YS=373.806 MPa, C=4016 MPa, and γ=94. It is concluded that the optimization process gives more consistency in the bending process.

Keywords: Chaboche model; Kinematic hardening; Optimization; Low cycle loading; Plasticity

1. Introduction

The drag link is one of the most important parts of the steering system. It is also called a drag link. It conveys movement from steering to tires. These parts are used for cars and for heavy vehicles, so they are crucial in the industry [1]. In Figure 1, a drag link and its components are shown. For assembling rod ties to the vehicles, a bending process is used. When road and driving conditions, they convey movement to the tires. Therefore, for proper assembly, an appropriate bending force is essential. The most effective tool to predict process parameters is finite element simulations of the deformation processes. There are two types of hardening rules mainly as isotropic and kinematic hardening rules. Both can be combined. Also both cam be linear or nonlinear. Drag links are used extensively as load-carrying parts in steering systems in automotive vehicles. Any fault in the angle of the drag link leads to poor results.

As seen in the figure, the bending angle is very important during use. Plasticity theories are used to determine the amount of plastic deformation (ε^p) in deformation process simulations. The total deformation in a body is decomposed as the summation of elastic (ε^e) and plastic (ε^p) deformation. The elastic part of the deformation can be obtained using elastic or hyperelastic constitute equations. However, the determination of the plastic part of the deformation requires a flow criterion, a hardening rule, and ultimately a flow rule. Chaboche's hardening model is a type of kinematic hardening rule.
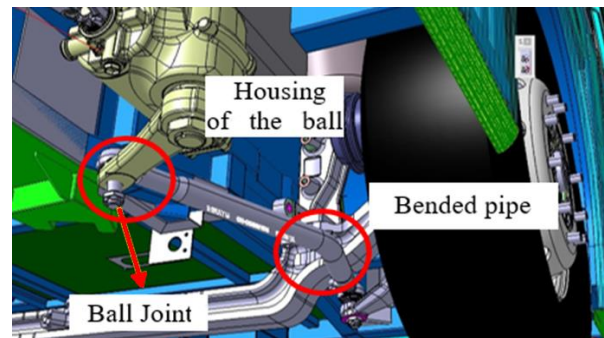

Fig. 1. Drag link and its components and usage area on the vehicle body

Linear kinematic hardening was first added into simulations by Prager's hardening rule [2] and then revised by Ziegler [3]. These linear hardening plasticity models are not sufficient to predict the Baushinger effect, multiaxial ratcheting, and plastic strain accumulation (shakedown). Therefore, nonlinear kinematic models were developed based on Armstrong and Frederick's equation [4]. Armstrong and Frederick's rule includes a strain hardening and recovery term in their equation. Then, in studies based on changing the term of dynamic healing in the formula of Armstrong and Frederick, many hardener plasticity models such as Chaboche have been developed [5, 6].

To date, no systematic method for the determination of material constants of a material's kinematic hardening models has not been developed. However, the model parameters are derived from a series of tension- compression, strain-controlled tests, and symmetrical or unsymmetrical loads at different strain amplitudes. Later, model parameters are fitted mathematically using curve fitting algorithms based on nonlinear regression.

In industry, the importance of pipe bending in general is increasing day by day. Steel drag links are used in the structure as load-carrying components [7,8]. Nowadays, welding with grinding and grinding takes a long time and is seen as heavy quality. Although this method was seen as an alternative, it is no longer useful. Pipe bending principles are used not only for round pipes but also for wires and hollow bars and oval, square, and rectangular profiles [9].

In the design and optimization of automotive components, an accurate prediction of material behavior subjected to complex loading conditions is essential. While isotropic hardening models account for material hardening due to plastic strain, they fail to capture the phenomenon of kinematic hardening, which describes the shift in the yield surface due to plastic strain history. This effect, commonly known as the Bauschinger effect, is crucial in automotive applications involving cyclic loading, such as engine components, suspension systems, and vehicle body structures [10]. In the sheet metal forming, which is an automotive application, the Armstrong-Frederick model is commonly used due to its simplicity and ability to capture the Bauschinger effect and strain-hardening behavior [11]. In the fatigue analysis, which is an automotive application, the Chaboche model is often preferred for its ability to capture complex loading histories and fatigue crack initiation behavior [12]. In the fatigue analysis, which is an automotive application, the Chaboche model, with its ability to model ratcheting, proves valuable for simulating large plastic deformation under impact conditions [13]. The Y-U model (Yoshida and Uemori, 1988) is a versatile model that utilizes a non-linear kinematic hardening rule based on the concept of back-stress evolution for different automotive materials, including steel, aluminum, and composites [14].

In this study, the Chaboche's nonlinear kinematic hardening rule's parameters for St52 alloy are determined by applying curve fitting methods on the tension–compression test data for use in the finite element simulation of the pipe bending process of the drag link. Furthermore, the Chaboche model parameters were calibrated by an optimization process. Finally, directional deformation at the punch movement direction and springback is measured experimentally and compared with those obtained from the optimized model. Therefore, a comprehensive methodology is presented for the determination of Chaboche kinematic hardening model's parameters for the bending of the pipe made from St52 material.

2. Material and Method

As material, St52 alloy is used. Its elemental content is given in Table 1.

Table 1. Chemical composition (%) of the St52 alloy

C	Si	Mn	P	S	Cr	Ni	Mo
0.19	0.406	1.37	0.018	0.0072	0.04	0.08	0.015
Al	**Cu**	**Co**	**Ti**	**Nb**	**V**	**W**	**Pb**
0.047	0.04	0.005	<0.001	<0.003	<0.001	0.025	<0.0030
B	**Sn**	**Zn**	**As**	**Bi**	**Ca**	**Ce**	**Fe**
<0.0005	0.0085	0.0044	0.008	<0.0020	0.0005	<0.0030	<97.7

There are several reasons why this steel grade is a favorite in this demanding sector such as excellent strength-to-weight ratio, high yield strength, good weldability, cost-effectiveness, and durability and resistance. St52 finds its way into various automotive parts such as chassis frames, axles and suspension components, engine mounts and brackets, body panels. However, St52 might not always be the ultimate choice. Other steel grades or even alternative materials like aluminum or composites might be preferred in specific situations depending on the specific requirements and weight restrictions.

The method followed in this study is given in Figure 2 schematically. It shows a plasticity model and its parameters.
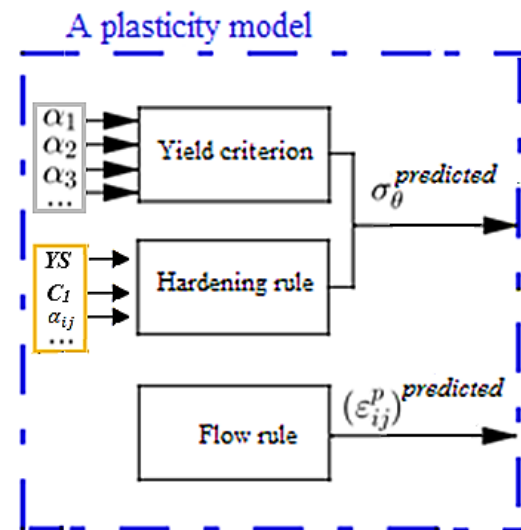

Fig. 2. Schematic representation of a plasticity model

2.1. Monotonic Tensile Test

A tensile test machine was used to determine the mechanical properties of the St52 alloy. Anisotropy coefficients are determined from literature [15].

Rectangular dog-bone-shaped specimens were prepared following the ASTM E8 standard. The geometry and dimensions of the specimen are shown in Figure 3a.
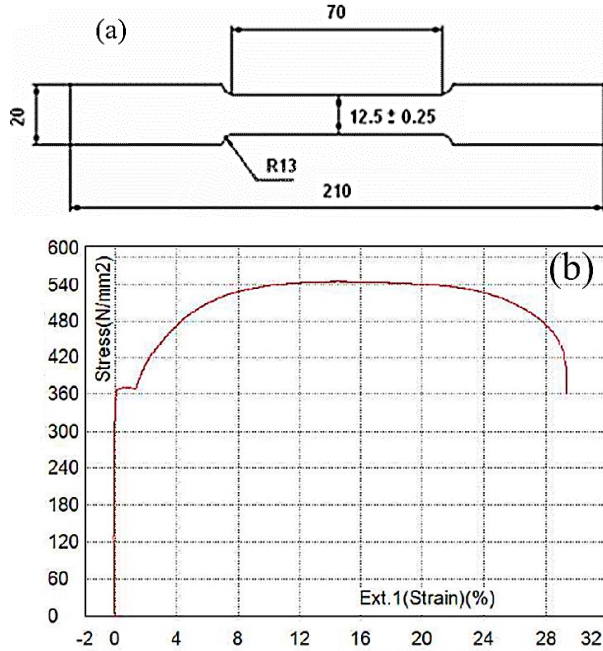

Fig. 3. a) Specimen dimensions for monotonic tensile test (in mm), b) test data

Tensile tests were performed on a Shimadzu Autograph 100 kN testing machine with a data acquisition system maintained by a digital interface board using a specialized computer program. Material deformation is measured using a video-type extensometer measurement system. The tensile tests were performed at 25 mm/min (0.0083 Hz) strain rate at room temperature. The curve of monotonic tensile test is shown in Figure 3b. It includes the true stress and true total strain.

Table 2. Mechanical properties of St52 steel

Property	Value
Density	7.85 gr/cm³
Young modules	207 GPa
Poisson ratio	0.28
Yield strength	373.806 MPa
Max. strength	414 MPa
r_0 [11]	0.791
r_{45} [11]	0.791
r_{90} [11]	0.804

2.2. Low Cycle Fatigue Test

Low cycle fatigue tests give curve(s) called hysteresis loop(s). Since these curves exhibit the difference between tension-compression paths, they are also used to determine the hardening model parameters. In fact, one loop is sufficient to determine the Chaboche model parameters, *YS*, *C*, and *γ*.

The test was performed using strain-controlled method at room temperature. Symmetric amplitude was applied. The dimensions of the samples are shown in Figure 4a. The holes on the specimen guarantee cantilever supporting and avoid buckling during compression strokes especially.
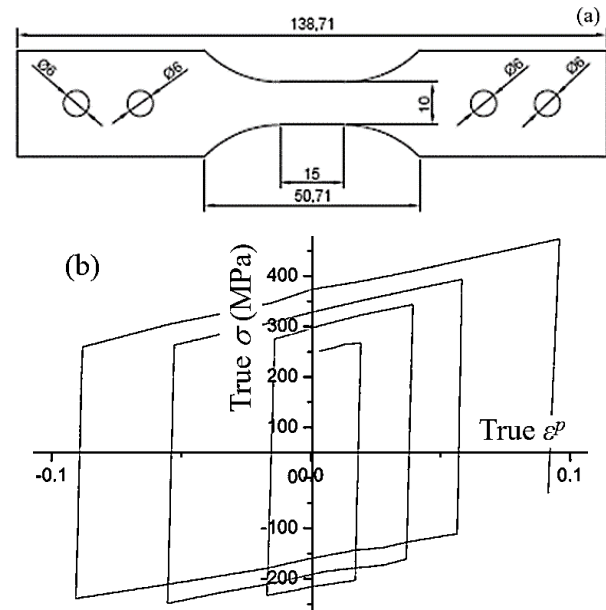

Fig. 4. a) Test specimens b) low cycle fatigue test data (3 loops)

Figure 4b shows three-stable loops. Since the deformation is low in the pipe bending process, only the innermost loop in the graph is used. The diagram includes the true stress and true plastic strain where elastic portion is subtracted. The deformation ranges are ± 0.08, ±0.06, ±0.03, ±0.05 (strain ratio $R = -1$). The test is conducted at a strain rate of 1 mm/min (0.0011 Hz). The Shimadzu-Autograph 100 kN tensile testing machine was also utilized to perform this test. The Bauschinger effect is the reason for the difference in hardening behavior in the tensile and compression zones.

The experimental data were pre-processed to remove the roughness and to obtain a smooth curve.

In this study, one-termed Chaboche hardening rule is used. Its parameters are $\{YS, C, \gamma\}$. Table 3 shows their raw values calculated by regression. Nonlinear regression is performed on this loop data. The "pre-processor→material Props→materials models→structural→nonlinear→inelastic-plastic curve fitting" module in the mechanical APDL module of Ansys© is used for the regression. Initially, the parameters were set to a value of 1. The maximum number of iterations was limited to 1000 in order to control the computational process. Additionally, normalized

error, residual, and coefficient tolerance were utilized as additional criteria to stop the iterations. In order to achieve the best fit, the goals for these criteria were set to zero. For the error minimization, the Levenberg-Marquard's optimization algorithm was employed. The confidence level for the fitting curves was set at 95%, ensuring a reliable estimation of the results. After the regression, the raw parameters are calculated as in Table 3.

Table 3. Chaboche's model's raw parameters

YS (MPa)	C (MPa)	γ
373.806	4016	94

2.3. Constitutive Equation

The constitutive equation, also called the plasticity model, consists of a yield criterion, a hardening rule, and a flow rule. In this section, the plasticity model used in this study is explained.

Yield Criterion: The yield criterion of Hill48 is employed. Its function is given in Eq. (1) for a general stress state case [16].

$$\Phi(\sigma_{ij}) = F(\sigma_{yy} - \sigma_{zz})^2 + G(\sigma_{zz} - \sigma_{xx})^2 + H(\sigma_{xx} - \sigma_{yy})^2 + 2L\sigma_{yz}^2 + 2M\sigma_{zx}^2 + 2N\sigma_{xy}^2 = \bar{\sigma}^2 \quad (1)$$

where Φ is yield function. When principle stress is used, the function for this criterion is given in Eq. (2).

$$\Phi(\sigma_{ij}) = F(\sigma_2 - \sigma_3)^2 + G(\sigma_3 - \sigma_1)^2 + H(\sigma_1 - \sigma_2)^2 - \bar{\sigma}^2 = 0 \quad (2)$$

where $\bar{\sigma}$, is the equivalent stress expression of the yield criterion. In Eq. (2), G, H, F, and N are coefficients. They can be calculated using experimental r_0, r_{45}, r_{90} values as given in Eq. (3).

$$F = \frac{r_0}{r_{90}(r_0 + 1)}, \quad G = \frac{1}{r_0 + 1}, \quad H = \frac{r_0}{r_0 + 1}, \quad N = \frac{(r_0 + r_{90})(1 + 2r_{45})}{2r_{90}(1 + r_0)} \quad (3)$$

When substituting for r_0=0.791 and r_{45}=0.791 and r_{90}=0.804, these coefficients are calculated as follows:

- F=0.35509
- G=0.55835
- H=0.44165
- N=1.42999

In Ansys©, a user-defined result-tool for Hill48 criterion including principle stress is given as;

((0.44165*(s1-s2)^2+0.355*(s2-S3)^2+0.55835*(s3-s1)^2))^0.5

Hardening Rule: Eq. (4) includes both kinematic (α_{ij}) and isotropic (σ_h) hardening rules. In this study, only Chaboche rule is used. Therefore $\sigma_h = 0$. The term, α_{ij} is called back-stress. It shifts the yield surface center to α_{ij}. Thus, different hardening behaviour are possible in the tensile and compression zones.

$$\bar{\sigma}(\sigma_{ij} - \alpha_{ij}) - \sigma_h = 0 \quad (4)$$

Some α_{ij} functions are suggested by Prager, Armstrong-Frederic, Chaboche, Yoshida-Uemori etc. In this study, the back stress equation of Chaboche is used as given in Eq. (5).

$$(\dot{\alpha}_{ij})_m = \underbrace{\frac{2}{3} C_m \dot{\varepsilon}_{ij}^{\;p}}_{lineer\;terim} - \underbrace{\gamma_m (\alpha_{ij})_m \sqrt{\frac{2}{3} \dot{\varepsilon}_{ij}^{\;p} : \dot{\varepsilon}_{ij}^{\;p}}}_{recall\;term} + \underbrace{\frac{1}{C_m} \frac{\partial C_m}{\partial T} (\alpha_{ij})_m \dot{T}}_{Isitma\;hizi\;terimi} \quad (5)$$

$$m = 1, 2, ..., n$$

where, T is temperature, C_m is hardening module and γ_m are the coefficients of the hardening reduction. These parameters may be different for each term. All of these parameters are determined in the same regression process. Although any curve is enough for regression, one hysteresis loop obtained from low cycle fatigue test must be employed.

Chaboche's back-stress equation is a first-order ordinary differential equation. If this differential equation is integrated explicitly according to ε_{ij}^p for the one-termed case (first-order), and no change in temperature, Eq. (6) will be achieved:

$$\alpha = \varphi \frac{C}{\gamma} + \left(\alpha_0 - \varphi \frac{C}{\gamma}\right) e^{-\varphi\gamma(\varepsilon^p - \varepsilon_0^p)} \quad (6)$$

In the equation, α_0 is initial back-stress value, ε_0^p is the initial plastic deformation value, φ is the sign depending on the tension/compression cases, $\varphi = sgn(\sigma - \alpha) = \pm1$. In the case of uniaxial tensile, $\varphi = 1$ while $\varphi = -1$ in the case of compression. In uniaxial tensile tests, assume the initial back-stress $\alpha_0 = 0$ and the initial plastic deformation $\varepsilon_0^p = 0$. Under these circumstances, the back-stress equation is given by Eq. (7).

$$\alpha = \frac{C}{\gamma}\left(1 - e^{-\gamma(\varepsilon^p)}\right) \text{ in the tension stroke} \quad (7a)$$

$$\alpha = \frac{C}{\gamma}\left(-1 + e^{\gamma(\varepsilon^p)}\right) \text{ in the compression stroke} \quad (7b)$$

The Chaboche equation gives α_{ij}. It is necessary to substitute it in the equivalent stress equation of the yield criterion as $\bar{\sigma}(\sigma_{ij} - \alpha_{ij}) - \sigma_0 = 0$ where σ_0 is the initial yield strength. In the case of uniaxial tensile, since the stress value in the tensile axis is already the principle stress, the equivalent stress in the uniaxial tensile will also be equal to the tension in the main axis x as $\bar{\sigma}(\sigma_{ij} - \alpha_{ij}) = \sigma_x$ In this case, the equivalent stress is expressed as in Eq. (8):

$$\bar{\sigma}(\sigma_x - \alpha_x) = 0 \quad (8a)$$

$$\sigma_x - \alpha_x = 0 \quad (8b)$$

If Eq. (7) is substituted to Eq. (8), then the stress value will be added to the yield criterion function (Eq. 9).

$$(\sigma_x)_t = \frac{1}{2} + \frac{C}{\gamma}\left(1 - e^{-\gamma(\varepsilon_x^p)}\right) \text{ in the tension stroke} \quad (9a)$$

$$(\sigma_x)_c = -\frac{1}{2} + \frac{C}{\gamma}\left(-1 + e^{\gamma(\varepsilon_x^p)}\right) \text{ in compression stroke} \quad (9b)$$

Flow Rule: A flow rule is required to calculate the plastic strain increment, $d\varepsilon_{ij}^p$, and its direction. It gives the relationship between plastic strain and stress. There are two types of rule as

325

associated flow rule and non-associated flow rule. The general equation of a flow rule is given in Eq. (10).

$$d\varepsilon_{ij}^p = d\lambda \frac{\partial f}{\partial \sigma_{ij}} \qquad (10)$$

where λ is called the plastic multiplier. f is a scalar function and is also called the plastic potential. If the yield parameter is taken as the potential function, this equation is called associated-flow rule. Otherwise, it is called a non-associated flow rule. While the associated flow rule is good at metals, a non-associated flow rule is used in the modelling of soil material.

2.4. Pipe Bending Experiments

In this process, the bending angle is increased. The drag-link pipe and its bending process are shown in Figure 5. A raw pipe is shown in Figure 5a. Bending is performed on the pipe inserted between the punch and supports as in Figure 5b. After bending, the pipe is transferred to a subsequent process called frettage and shrinking. In frettage, inner parts (ball joints) are inserted into the just shrunken end to finalize the mounting process (Figure 6). These sequences cause the pipe material to be strain hardened due to plastic flow. This study focuses on the bending step only.
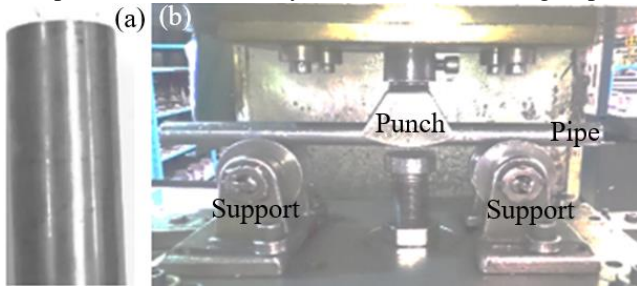

Fig. 5. (*a*) Initial pipe and (*b*) bending process of the drag link pipe

Fig. 6. Drag link's pipe after bending on which assembled components

At the beginning, the drag link pipe's outer diameter is $\phi 52$ mm, thickness is 7 mm, and bending angle is 0°. After bending, the bending angle increases up to 16,6°. This deformation causes large deflection in the pipe geometry. In the finite element simulation, frictional contacts must be set between the pipe and punch surfaces. To provide permanent deformation on the drag link pipe, the analysis must include a plasticity model. Frictional contact, large deflection, and permanent deformation lead the analysis to nonlinear simulation.

3. Simulation

3.1 Bending Simulation

Using ANSYS© software, the bending process is simulated based on finite element method where a quarter model is used for convenience because the geometry includes two-planar symmetricities. *x-y* and *x-z* planes are the two-symmetry planes. The punch is linearly moved toward the pipe body, as seen in Figure 7. First, a dynamic analysis to deform the pipe is performed. Later, using it, an optimization is performed for Chaboche's model's parameter's calibration. A remote displacement boundary condition (BC) is applied to the support point given in the figure where displacements in the *x*-component=0 and *z*-component=0 while other degrees of freedom (DOF) are free.
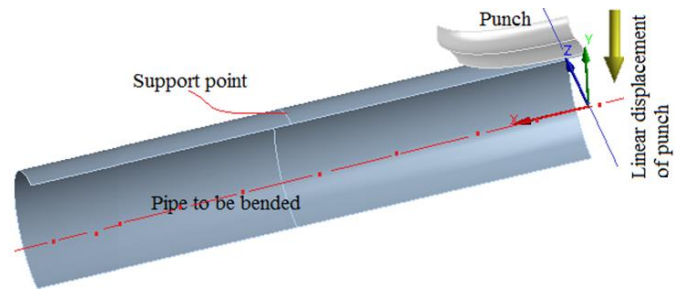

Fig. 7. A quarter-symmetric model of the pipe bending process

As given in Figure 8, another displacement load history on the punch is applied in the *y*-direction where the displacement in *z* and *x*-directions are set to zero. For the pipe to avoid out-of-plane movement, another displacement BC is applied on the middle point of the pipe where *z*-component of the displacement is set to zero while other DOFs are free.
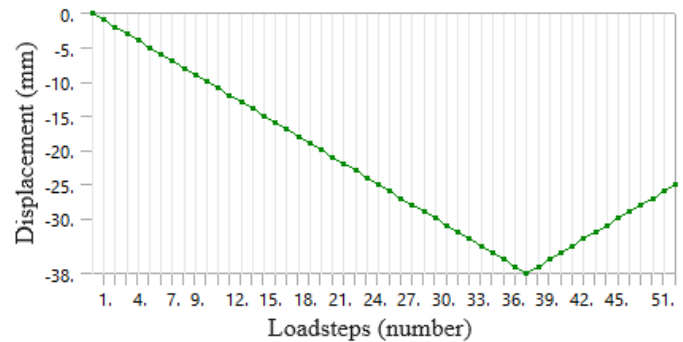

Fig. 8. Applied load history

The friction coefficient between the punch and pipe is set as 0.125. The punch is modelled as a rigid body to decrease calculation time. The pipe is a flexible body assigning with St52 material. While elastic properties in Table 2 is used for both bodies, plastic properties in Table 3 are assigned to the pipe body.

At the beginning, a mesh independence analysis is performed to determine the optimum mesh size. The mesh independence analysis is based on the equivalent stress as seen in Table 4.

Table 4. Mesh independence analysis

Element size (m)	Ele-ment counts	Stress (MPa)	APE (*) (%)	Compu-tation time (s)	Memory (MB)	Result file size (MB)
0.006	583	144.4	--	620	16.03	30.27
0.005	809	155.0	0.0688191	1240	48.18	43.91
0.004	1283	167.4	0.073713	1860	48.89	57.52
0.003	1777	181.8	0.0793401	1860	51.19	86.29
▶ 0.003	2235	165.2	0.100334	2480	53.50	118.07
0.003	2989	165.2	0.0000000	4960	55.71	145.31
0.002	4864	165.2	0.0000000	6200	58.10	192.25
0.002	6213	165.2	0.0000000	8681	58.90	305.76
0.001	10118	165.2	0.0000000	11781	84.05	392.05

(*) Absolute value of relative percent error

It is seen that the stress results don't change significantly after 2235 elements. So, the model with 2235 elements is selected as an optimum element count. The simulations were performed on a computer having 3.40 GHz quad-core CPU and 8 GB RAM.

3.2. Optimization using Bending Simulation

The mathematical meaning of optimization is to find the maximum, minimum, root, or any desired value of a function. In the optimization process, the goal is to find the Chaboche coefficients, YS, C, γ, which lead to the most accurate bending angle results from the simulation.

The design point to give the bending angle nearest the experimental measurements will be chosen as the best fit, namely candidate point(s). Finally, candidate points are verified using in the bending simulation.

The parameters are defined in Figure 9. The experimental measurements are given in Table 5.
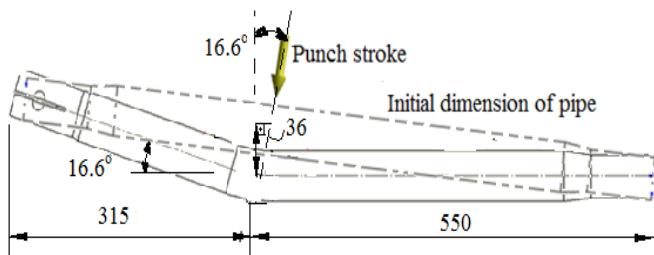

Fig. 9. Experimental dimension measurements after bending (in mm)

All experiments are performed on the pipe with 865-mm length and 52-mm diameter nominally. Distance between the support is 117.5 mm. The pipe having 6.888 mm thickness and 16.6° bending angle is selected for scoping.

In this study, the maximum directional deformation (at y-direction) obtained from the dynamic analysis simulation is parameterized. The upper and lower limits of the Chaboche coefficients are used, as shown in Table 6.

Table 5. Experimental measurements from the pipe bending process

Pipe thickness (mm)	Bending angle (°)	Punch stroke (mm)
6.889	16º40′	36.01
6.905	16º30′	36.01
6.907	16º25′	36.01
6.902	16º25′	36.01
▶ 6.888	16º60′	36.01
6.990	17º05′	36.01
6.995	16º35′	36.01
6.953	16º35′	36.01
6.905	16º35′	36.01
6.942	16º35′	36.01

Table 6. Lower and upper limits of design variables

	YS (MPa)	C (MPa)	γ
Initial values	373.806	4016	94
Lower bound	350	2500	10
Upper bound	450	4000	100

The optimization module calculates the 100 design points determined between the upper and lower limits. In addition, for all values among these points, the response function is determined, which is based on the curve fitting method.

For optimization, constraints are applied as follows:

- No constraint for YS,
- No constraint for C,
- No constrain for γ,
- For bending angle, seek 16.6°.

4. Results and Discussions

4.1. Response Surface of Optimization

The response surface graph is given in Figure 10 when initial values YS=373.806 MPa, C=4016 MPa, and γ=94 are used.
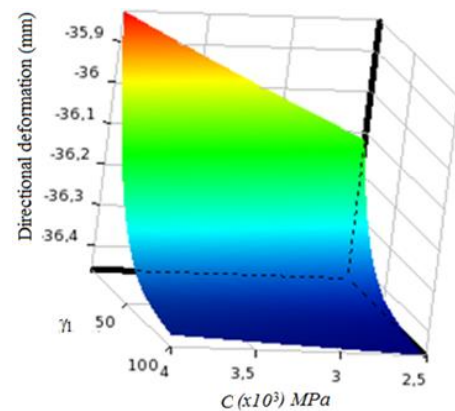

Fig. 10. Response surface

After 100 design points are calculated using simulation, the optimization module creates a response surface between all parameters.

The function for the response surface is fitted by the optimization process, and it needs to be verified. For verification, these values should be re-analysed as a new design point to determine if the difference between the calculation and the estimation value is reasonable. To obtain the bending angle, a user defined result is coded using the geometric relation between the angle and the directional deformation. The design points created by the optimization module and the stress values obtained at the end of the solution for each point are given in Table 7.

Table 7. Created design points and bending angle results for first 10 data

Number of design points	Input			Output
	YS (MPa)	C_1 (MPa)	γ	Bending angle (°)
1	445.6603349	2514.313487	10.24394162	15.99003983
2	350.3548682	2877.601439	11.95790706	16.21468735
3	447.4784572	3882.623548	10.48864854	15.71844864
4	448.7009859	2510.884541	91.21224601	16.33758163
5	407.9422143	3622.064395	84.65095669	16.40490341
6	366.2731693	3996.223957	15.86404091	16.0661087
7	370.9312172	2501.451917	79.39028227	16.53705597
8	406.0529985	3134.148596	34.67077987	16.30681229
9	448.9464196	3523.884859	53.43458643	16.24684525
10	356.1461818	3422.637651	43.05057767	16.42939377

4.2. Optimum values

As a result, the optimization module suggests the optima as given in Table 8. Four optimization methods are employed such as MOGA (Multi-Objective Genetic Algorithm), NLPQL (Nonlinear Programming with Quadratic Lagrangian), MISQP (Mixed Integer Sequential Quadratic Programming) and screening.

Table 8. Candidate point for optimal results

Optimization Method	C (MPa)	γ	YS (MPa)	Bending angle (°)
Screening	2500	100	350	16.588
MOGA	3816.3	16.77	404.54	15.999
NLPQL central difference	2984.3	100	350	16.579
MISQP-forward difference	2984.3	100	350	16.579
MISQP-central difference	2984.3	100	350	16.579

However, these values are obtained from the response surface by the optimization tool. They need to be verified by re-simulating. The verification results are given in Table 9.

Table 9. Verified results

Optimization Method	C (MPa)	γ	YS (MPa)	Bending angle (°)	APE (*)
Screening	2500	100	350	16.61	%0.06
MOGA	3816.3	16.77	404.54	16.029	%0.08
NLPQL central difference	2984.3	100	350	16.579	%0.04
MISQP-forward difference	2984.3	100	350	16.579	%0.04
MISQP-central difference	2984.3	100	350	16.579	%0.04

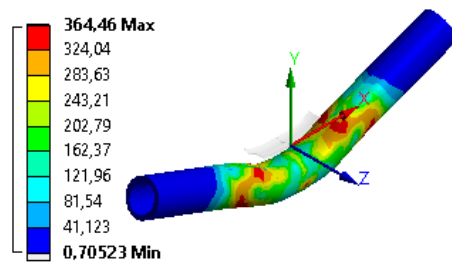(*) Absolute value of relative percent error based on the reference (16.6°)

As seen from tables, NLPQL and MISQP provide the best fit where YS=350 MPa, C=2984.3 MPa, and γ=100.
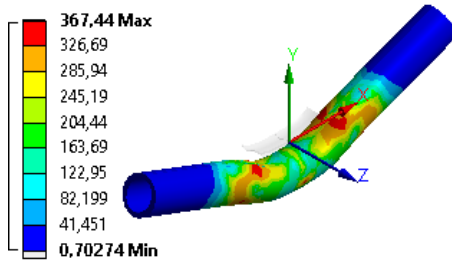
4.3. Stress and strain responses

The Von Mises stress, which is another well-known yield criterion, was compared with the Hill48 stress by analysing the results obtained from the solution in the final sub step of the last step. As depicted in Figure 11, the Hill48 stress slightly surpasses the Von Mises stress.

Von Mises theory is simpler, easier to calculate. It is good at isotropic materials, but less accurate at anisotropic materials. It has wide range of applications for ductile materials. However, Hill48 theory is more complex, requires anisotropic parameters as well. It is good at anisotropic materials. It is more specific, suitable for materials with direction-dependent properties. In the present study, the pipe material, St52, has ductile behaviour. Also anisotropy coefficients F, G, H, N of Hill 48 are very close to 0.5. Note that Hill48 turns to Von Mises when F=G=H=0.5. It shows that both Von Mises and Hill48 are suitable for preliminary study for this case. Already, the results in figure are close for both. It can be concluded that the pipe bending process doesn't show significant anisotropy. However, anisotropy is inherently present due to rolling process in all sheet metals even tubular pipe. So, Hill48 is suggested although Von Mises is good at in this study, as well.

The central part of the pipe experiences the highest stresses, attributed to the flow separations in opposite directions. In contrast, the stress at the bottom end of the pipe is relatively lower, as the material flows towards the free ends. Beyond the support points, no stress is seen as expected because of free movement. Figure 12 shows deformation results.

(a) Units are in MPa

(b) Units are in MPa

Fig. 11. (*a*) Von Mises (*b*) Hill48 stress distribution on bended pipe body when *YS*=350 MPa, *C*=2984.3 MPa, and γ=100
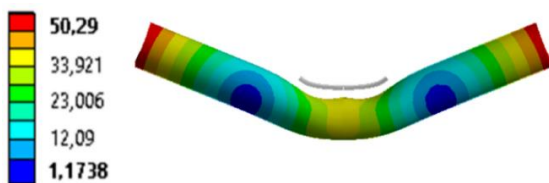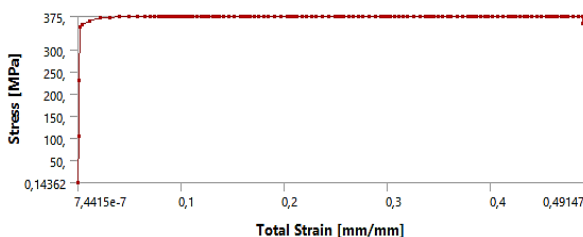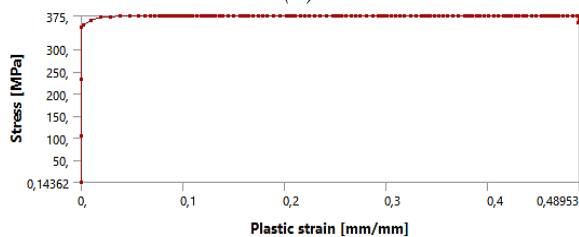

Fig. 12. Deformation results (mm) obtained when *YS*=350 MPa, *C*=2984.3 MPa, and γ=100

The total and the plastic only strain and stress responses of the material collected from simulation are given in Figure 13 when optimum material parameters are used.

(a)

(b)

Fig. 13. Stress versus a) total, b) plastic strain

Also, Figure 14 gives the deformation results when the initial parameters are used.
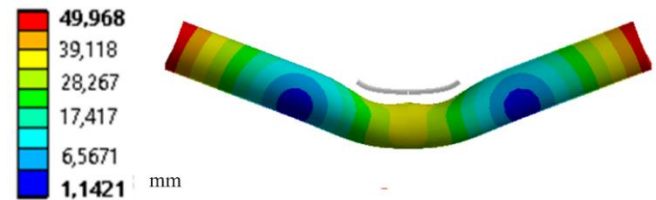

Fig. 14. Deformation results obtained when *YS*=373.806 MPa, *C*=4016 MPa, and γ=94

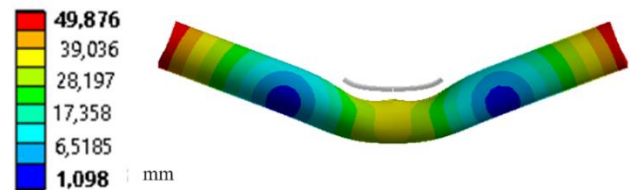Figure 15 gives the deformation results when *YS*=404.54 MPa, *C*=3816.3 MPa, and γ=16.766 are used.

Fig. 15. Deformation results (mm) obtained when *YS*=404.54 MPa, *C*=3816.3 MPa, and γ=16.766

Figure 16 gives the deformation results when *YS*=350 MPa, *C*=2984.3 MPa, and γ=100 are used.
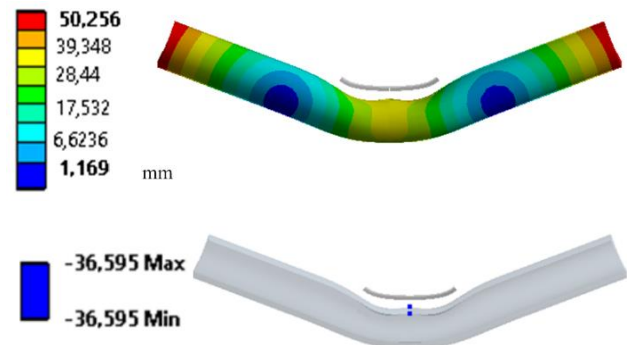

Fig. 16. Deformation results (mm) obtained when *YS*=350 MPa, *C*=2984.3 MPa, and γ=100

4.4. Industrial applications of the optimization methods

MOGA method is good at product design optimization, supply chain optimization, and resource allocation. NLPQL may be chosen in portfolio optimization, production planning, and resource allocation. MISQP is good at production planning, transportation logistics which optimizing transportation routes with mixed integer variables for load assignment and route selection. Also it may determine the optimal location for facilities, considering both continuous variables like coordinates and integer variables for facility size and capacity. The screening method is

good at product design selection, materials selection and process optimization.

As can be seen, all methods have lots of ability. So, how can the right method be selected? The best optimization method for a specific scenario depends on factors such as problem type (linear/nonlinear, convex/non-convex, constrained/unconstrained), objective function (the complexity and differentiability of the objective function), number of variables (the dimension of the search space), computational resources (available processing power and memory), and accuracy requirements (the desired precision of the solution).

In conclusion, each method offers unique strengths and weaknesses, and the best approach often involves combining different techniques. Understanding the nature of the problem, its constraints, and the desired outcomes will guide you in choosing the most appropriate optimization method for successful results.

5. Conclusions

Due to Hill48 yield criterion's ease of use, it is one of the most popular anisotropic yield criteria used in plastic deformation processes. In this study, pipe pending process is simulated. As the plasticity model Hill48, Chaboche, and associated flow rules are used. To determine their parameters, low cycle fatigue test is performed. Applying nonlinear regression, Chaboche's parameters are determined. Chaboche's kinematic hardening rule parameters are optimized for St52 alloys. The optimization provides an inverse analysis technique. Five optimization methods are used such as screening, MOGA, NLPQL central difference, MISQP-forward difference, MISQP-central difference. The main results obtained from these studies are as follows:

• The most consistent results are obtained by the NLPQL and MISQP methods. Both methods are simple and easy to implement. Also it is effective for large datasets. Moreover, the method is fast and efficient.

• The success of NLPQL and MISQP strongly depends on the initial values or ranges. NLPQL is good at convex problems. It handles linear and nonlinear constraints. It has well-established theory. NLPQL has a strong theoretical foundation, which ensures its reliability. However, it is limited to convex problems: NLPQL might struggle with non-convex problems, potentially getting trapped in local optima. It is sensitive to initial values. It typically requires the objective function and constraints to be differentiable. MISQP is strong to handle mixed integer variables. It is efficient for constrained problems. It provides local optima. However, it may struggle with non-convex problems. Its computational intensity is high, especially for large-scale problems. It works best with problems that have specific structures and can be formulated as quadratic programming problems.

• The optimum parameters are YS=350 MPa, C=2984.3 MPa, and γ=100 while the raw values are YS=373.806 MPa, C=4016 MPa, and γ=94. It is concluded that optimization process gives more consistency with respect to bending process.

• The optimization module calculated the response surface function which has accurate predictions.

• This study has future work potentials to investigate the combined hardening rules with more terms.

Conflict of Interest Statement

The authors declare that there is no conflict of interest in the study.

CRediT Author Statement

Ozan Akkoyun: Review, Data curation, Formal analysis, Writing-original draft-editing, Validation, Simulation
İlyas Kacar: Review, Conceptualization, Reading-original draft, Validation.

References

[1]. Ortego A, Calvo G, Valero A, Iglesias-Embil M, Valero A, Villacampa M. Assessment of strategic raw materials in the automobile sector. Resources, Conservation and Recycling. 2020; 161:104968. https://doi.org/10.1016/j.resconrec.2020.104968

[2]. Prager W. Recent developments in the mathematical theory of plasticity. Journal of Applied Physics, 1949; 20(3):235-241. https://doi.org/10.1063/1.1698348

[3]. Ziegler H. A modification of Prager's hardening rule. Quarterly of Applied Mathematics, 1959; 17(1):55-66. https://doi.org/10.1090/qam/104405

[4]. Armstrong PJ and Frederick CO. A mathematical representation of the multiaxial Bauschinger effect. Materials at High Temperatures, 2007. 24(1) p. 1-26. https://doi.org/10.3184/096034007X207589

[5]. Chaboche JL. Time independent constitutive theories for cyclic plasticity. International Journal of Plasticity, 1986; 2(2): 149-188. https://doi.org/10.1016/0749-6419(86)90010-0

[6]. Chaboche JL. Constitutive equations for cyclic plasticity and cyclic viscoplasticity. International Journal of Plasticity, 1989; 5(3): 247-302. https://doi.org/10.1016/0749-6419(89)90015-6

[7]. Mahdi MS, Mohammed AI. The effect of bending angle and radius on wall thickness variation according to a geometric ratio in tube bending. AIP Conf. Proc. 19 August 2024; 3105 (1): 020024. https://doi.org/10.1063/5.0212722

[8]. Duan W, Joshi S. Structural behavior of large-scale triangular and trapezoidal threaded steel tie rods in assembly using finite element analysis. Engineering Failure Analysis. 2013;34:150-65. https://doi.org/10.1016/j.engfailanal.2013.07.024

[9]. Falah AH, Alfares MA, Elkholy AH. Failure investigation of a tie rod end of an automobile steering system. Engineering Failure Analysis. 2007; 14(5): 895-902. https://doi.org/10.1016/j.eng-failanal.2006.11.045

[10]. Lubarda VA. Elastoplasticity theory. 2002, CRC Press, 56-68. https://doi.org/10.1201/9781420040784

[11]. Aretz H, Groche P, Schindler K. Modeling of sheet metal forming processes with kinematic hardening. International Journal of Plasticity, 2002, 18(4), 453-475. https://doi.org/10.1007/s12289-008-0035-y

[12]. Lemaitre J, Chaboche JL, Mechanics of solid materials. 1990, Cambridge University Press, 86-67. https://doi.org/10.1017/CBO9781139167970

[13]. Zhu X, Zhou S. A review of material constitutive models and their application in crashworthiness simulations. Materials, 2019; 12(19), 3141. https://doi.org/10.1201/9781003143031-16

[14]. Yoshida F, Uemori T. A constitutive model of cyclic plasticity for metals. International Journal of Plasticity, 1988; 4(4), 257-272. https://doi.org/10.1016/S0749-6419(99)00058-3

[15]. Xia QX, Xu T, Wei GM, Ye FY. Numerical Simulation and Experimental Research on Multi-position Progressive Stamping Process of Automotive Structural Part. Applied Mechanics and Materials. 2013; 271:1366-71. https://doi.org/10.4028/www.scientific.net/AMM.271-272.13

[16]. Zhang SY, Leotoing L, Guines D, Thuillier S. Calibration of material parameters of anisotropic yield criterion with conventional tests and biaxial test. Key Engineering Materials. 2013;554:2111-7. https://doi.org/10.4028/www.scientific.net/KEM.554-557.2111